

pubs.acs.org/cm Article

Design Rules to Optimize the Intermolecular and Long-Range Packing of Organic Semiconductor Crystals

Farahnaz Maleki, Karl J. Thorley, Hamna F. Iqbal, Daniel Vong, Toulik Maitra, Anthony Petty, Luke L. Daemen, Sean R. Parkin, Oana D. Jurchescu, John E. Anthony, and Adam J. Moulé*



Cite This: Chem. Mater. 2024, 36, 4794-4805



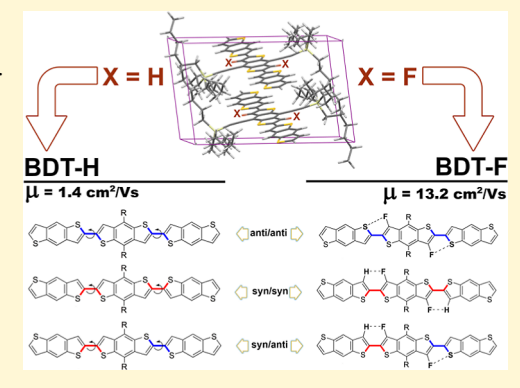
ACCESS I

III Metrics & More

Article Recommendations

s Supporting Information

ABSTRACT: Understanding the structure and configurations of small-molecule organic semiconductor (OSC) materials is essential in modifying their material properties. Here, we use density functional theory (DFT) to explore the impact of intramolecular noncovalent interactions on the isomerization and structure of the benzodithiophene (BDT) trimer. Fluorine substitutions modify the dihedral coupling between BDTs on the same molecule, thereby significantly increases charge mobility up to $13.2~{\rm cm}^2~{\rm V}^{-1}~{\rm s}^{-1}$. In the fluorinated isomers, the formation of hydrogen bonds overcomes the repulsive S···S interaction in the syn-conformer, leading to a more planar backbone structure. To validate the DFT simulations, we simulated inelastic neutron scattering (INS) spectroscopy of different anti- and syn-isomers in mixed configuration crystals and compared them to measured INS. Two main messages emerge from this study. (1) Although the through space interaction of fluorine with sulfur is the main contributor to dihedral planarization,



H-bonding formed through selective fluorination plays a critical role. (2) A crystal structure that includes a mixture of several configurations could have significant mobility, while the dihedral disorder is mitigated by configurations that are energetically very similar. Our investigation reveals that both syn- and anti-conformers are common in the BDT-trimer crystal, demonstrating that isomeric or configuration purity is not a prerequisite for high charge mobility over $10 \text{ cm}^2 \text{ V}^{-1} \text{ s}^{-1}$. This work provides a fundamental understanding of the interplay between intramolecular interactions, isomerization, and side chain effects in OSC materials, guiding the design of new generations of OSC materials.

■ INTRODUCTION

Organic semiconductors (OSCs) show tremendous potential for various applications such as photovoltaics, 1,2 organic lightemitting diode displays,³ flexible transparent electronics,⁴⁻⁶ and biocompatible medical devices. 7,8 The unique properties of OSCs have captured the attention of researchers in diverse fields, ranging from exploring charge transport mechanisms to synthesizing new OSCs using theory derived 9-11 and experimentally validated 12-14 design rules. Traditionally, OSCs can be broken into two distinct categories, small molecule materials with high crystalline order that, until recently, were exclusively vacuum processed¹⁵ and polymers with low crystalline order that are exclusively processed from a solvent.16 To harness the best properties of both material types, crystalline oligomers have recently been synthesized that combine long-range intermolecular crystalline order with longrange intramolecular delocalization along conjugated backbones. 17-19 For these oligomers, rigid planar molecular building blocks, consisting of multiring conjugated units such as benzodithiophenes (BDTs), are connected through freely rotating dihedral bonds. Just like in a polymer, the dihedral angle between neighboring BDT units controls the delocalization of ground states, polarons, and excitons. Like polymers,

oligomeric crystals are more structurally complex because neighboring BDT units in the same molecule can assume either syn- or anti-configurations depending on the relative position of sulfurs. Ideal molecular packing would combine large multiring backbone structures into perfectly organized and planar 3D structures with all anti- or syn-configurations. However, as the conjugated backbone becomes larger, entropy enables the incorporation of combined syn/anti configurations to become frozen into the same crystal, which should significantly increase the energetic disorder for charge transport. The use of selective fluorination has been proposed as a design motif that enhances backbone planarity and anti-configuration packing. The goals of this study are to examine protonated and selectively fluorinated BDT trimers, labeled BDT-H and BDT-F, respectively, and to determine whether and how much selective fluorination enhances

Received: March 4, 2024 Revised: April 19, 2024 Accepted: April 22, 2024 Published: May 5, 2024





Scheme 1. (a) BDT-H and (b) BDT-F Trimer Structures. (c) Showing the Dihedral Angles of the Anti (Blue) and Syn (Red) Orientations among the Backbones of the BDT Trimer and (d) S···F and H···F Intramolecular Interactions in the Anti- and Syn-Isomers of BDT-F Trimers, Respectively

backbone planarity and the ratio between syn- and anticonfigurations. The results described here are generalizable to a broad range of polymers and oligomers and should clarify design rules for the future synthesis of improved OSCs.

The presence of heteroatoms in the highly symmetric backbone of OSCs can lead to an isomeric mixture of products. Recent efforts have been made to understand how isomeric purity impacts material characteristics. Tykwinski and coworkers synthesized isomerically pure bis-trimethylsilyl-syndifluoroanthradithiophene (syn diF-TES-ADT). The resulting pure-syn thin-film transistors demonstrated comparable performance to devices with a mixture of syn- and antiisomers.²² In a separate study, films of pure-anti diF-TES-ADT were synthesized. In this case, the pure-anti film exhibited about 2× higher field effect hole mobility (μ_h) compared to a mixed syn/anti film. While the lower mobility measured in the mixed-isomer films was assigned to the higher trap density in the domains of isomer coexistence, 23-25 from these studies, it was not clear why the pure anti-configuration yielded improved $\mu_{\rm h}$ while a pure syn crystalline film did not. Similar results demonstrating high μ_h in mixed configuration films have been observed in unfunctionalized ADTs. 27,28 With the introduction of a dihedral bond into the backbone structure, it is important to consider that intramolecular interactions, specifically hydrogen bonding, play an important role in favoring synand anti-isomers. For instance, Wange and colleagues demonstrated the role of hydrogen bonding in thienyldiketopyrrolopyrrole (ThDPPTh) as a conformational constraint, resulting in the stabilization of the N,S-syn conformation of ThDPPTh.²¹

We were curious to explore the impact of combined structural and dynamic disorder on the hole mobility of crystalline OSCs. In particular, we hypothesized that breaking the typical rigid, fused aromatic chromophore into a series of smaller units linked by C–C single bonds might help diminish the role of long-axis vibrations on charge transport.²⁹ To that end, we developed a universal crystal engineering core based

on silylethyne-substituted BDT and optimized the crystal packing of the BDT trimer, Scheme 1a, to yield the 2-D "brickwork" molecular arrangement needed for high μ_h transistor applications.³⁰ After extensive optimization of surface treatments and deposition conditions, we were able to achieve a hole mobility (μ_h) slightly greater than 1 cm² V⁻¹ s⁻¹.30 This value was surprisingly low since the calculated electronic coupling based on the expected crystal packing was 202 meV, which would suggest that a substantially higher μ_h is possible. To improve the performance, we also explore the effect of selective fluorination of this material, as shown in Scheme 1b. Selective fluorination of conjugated organic molecules is a strategy that is used to increase backbone planarity between conjugated ring structures and thereby to enhance μ_h in OSCs. 31-33 S...F and H...F noncovalent interactions are attributed to the higher backbone planarity and increased mobility in conjugated polymers and OSCs.^{34–3} The presence of the fluorine could stabilize a planar synconfiguration via hydrogen bonding between the fluorine and neighboring proton or it could stabilize the anti-configuration through attractive S···F interactions. 38,39 For both configurations, we hypothesize that the attractive interaction will planarize the dihedral angle between neighboring rings and thereby increase delocalization of the polaron through the backbone and increase the μ_h . The measured μ_h of more than >10 cm 2 V $^{-1}$ s $^{-1}$ seems to validate our hypothesis but does not actually explain why the $\mu_{\rm h}$ increases because the fluorine stabilizes both syn- and anti-configurations. Thus, a molecular design rule that explains the role of fluorine substitutions in increasing $\mu_{\rm b}$ in mixed configuration crystals is still lacking. The detailed measurements and modeling in this article will provide this general design rule.

Recently, the Moulé group studies on OSCs have revealed that inelastic neutron scattering (INS) spectroscopy is a valuable tool for validating all phonon modes crucial for accurately calculating dynamic disorder and hole mobility in OSCs. 40,41 Compared to optical vibrational spectroscopy, INS

offers several advantages. It has no selection rules, enables measurement across a broader energy range, and accounts for momentum transfer. Descriptional sensitivity to proton-rich materials, enabling measurement of the weighted density of proton motions, which is exceedingly sensitive to intermolecular interactions. NS enables unprecedented accuracy in the measurement of phonon modes from 3 to 5000 meV. Coupled with density functional theory (DFT) simulations, INS can quantitatively validate the assignment of different molecular configurations and molecular defects. Alarm In addition, the combination of INS, DFT, and a dynamic delocalization transport model has yielded a more accurate prediction of $\mu_{\rm h}$ than any other method and even enables visualization of dynamic disorder for improved synthesis.

The BDT-H and BDT-F trimers studied here can assume several different polymorphs because of the two dihedral bonds and syn/syn, anti/anti, and anti/syn interactions with neighboring molecules. In addition, while the conjugated backbones form repeating crystals, the side chains assume a wide variety of quasi-amorphous configurations, which complicates the assignment of the INS spectrum and the use of plane wave DFT to solve the structure. This study explores both single molecule and plane wave crystalline simulations to account for the effects that molecular packing has on both structure and intermolecular electronic coupling. We show how the validation of simulations to INS data is a critical component for meaningful assignments.

■ METHODOLOGY

Experimental Methods. Recently, Anthony and coworkers reported a robust and straightforward approach to induce π -stacking in aromatic chromophores.³⁰ They achieved this by utilizing a universal aromatic core molecule that includes a trialkylsilylethynyl group to control the arrangement of the crystals. This method allows for the attachment of a wide range of π -conjugated pendants. For their study on optimizing crystal packing for organic field-effect transistor (OFET) applications, they focused on the BDT pendant and made a simple adjustment to the trialkylsilyl group, resulting in a champion material known as BDT trimer; see Scheme 1a. This remarkable material exhibited a hole mobility of 1.6 cm² V⁻¹ s⁻¹. The fluorinated trimer, Scheme 1b, was conveniently prepared following the methods developed for the preparation of Scheme 1a. The requisite fluorinated cores for Scheme 1b were synthesized in two steps from a BDT derivative reported by Yu and co-workers, 47 see Supporting Information for more details.

The INS spectra of both BDT-H and BDT-F trimers were measured using a VISION spectrometer located at Oak Ridge National Lab. INS spectrometers can be categorized into two types: indirect and direct geometries. Indirect geometry spectrometers do not directly measure the phonon modes or the currently active phonons. Instead, they provide the phonon density of states averaged over momentum (Q). On the other hand, direct geometry spectrometers measure the currently active motions and their Q-dependence. The VISION instrument used for these measurements is an indirect geometry neutron spectrometer. To enhance the accuracy of the measurements, the INS was measured at cryogenic temperatures (5 K). This reduced signal attenuation and broadening caused by the Debye—Waller effect and minimized the inherent noise from thermally activated phonons.

Transistor Fabrication and Characterization. Bottomcontact, top-gate OFETs were fabricated on substrates that have been first cleaned by immersion in an acetone bath, followed by an isopropyl alcohol bath (both for 10 min and maintained at 85 °C). Next, the substrates were exposed to UV-ozone for 10 min, rinsed with deionized water, and dried under a nitrogen gas. The source and drain electrodes (3 nm Ti and 40 nm Au) were deposited through a shadow mask and then chemically modified with pentafluorobenzenethiol (PFBT) self-assembled monolayer by submersion in a 30 mM solution of PFBT in ethanol for 30 min. Several different procedures have been explored for the deposition of the OSC film as well as for the OFET structure, and the results yielding the best device performance are detailed below. The BDT-H trimer films were spin-coated from a 1.5 wt % solution in chlorobenzene and then placed in a vacuum desiccator for 2 h to remove any residual solvents. A layer of parylene C (750 nm) was evaporated on top according to the procedure reported elsewhere to serve as a gate dielectric, 30,48 and a 50 nm Au film was then thermally evaporated through a shadow mask to form the top gate electrode. The BDT-F trimer films were spin-coated from a 1.5 wt % solution in 1,2,4trichlorobenzene and annealed on a hot plate at 100 °C for 15 min. To complete the top gate devices, a 1400 nm layer of Cytop (CTL-809-M) was spin-coated over the films, annealed on a hot plate at 100 °C for 20 min, and placed in a vacuum desiccator overnight at room temperature. A 50 nm layer of Au was thermally evaporated through a shadow mask as a top gate

OFETs were electrically characterized using an Agilent 4155C Semiconductor Parameter Analyzer. All measurements were performed in the dark, at room temperature, and in ambient air. The charge-carrier mobility was determined from the slope of the $\sqrt{I_{\rm D}}$ vs $V_{\rm GS}$ plot in the saturation regime. ⁴⁹ At least 20 devices of each type have been measured, and the results were consistent.

Computational Methods. In this work, we studied both molecular systems and crystalline solids. Thus, we utilized two different computational approaches and electronic structure codes. For the investigation of frontier molecular orbitals, we employed the Gaussian code, ⁵⁰ making use of a local Gaussian-type atomic orbital basis set. For the study of isomers in the periodic system as well as phonon calculations, we adopted the periodic VASP code, ^{51–53} based on plane wave and supercell approaches. The details of the computational setup are provided in the Supporting Information.

Supercell Calculations. For the calculation in the periodic system, we used the crystallographic information file (CIF) of BDT-F: CCDC 2346983. By replacing F atoms with H, we found the BDT-H structure. The CIF was the initial structure in obtaining the related isomers, as shown in Figure 3. We optimized the unit cell parameters and the atomic geometry of the crystalline structures for all isomers. The structural data of the most stable isomers are detailed in Tables S3-S6. Based on our previous studies, it has been shown that DFT calculations, although requiring much greater computational time than other methods, produce an excellent agreement between the simulated results and experimental data of INS spectra.⁵⁴ Based on this finding, the calculations of the periodic system have been performed using the VASP 5.4.4 package. 51-53 The valence electrons (H (1s), C (2s, 2p), F (2s, 2p), Si (3s, 3p), and S (3s, 3p)) are expanded on a set of plane waves with a

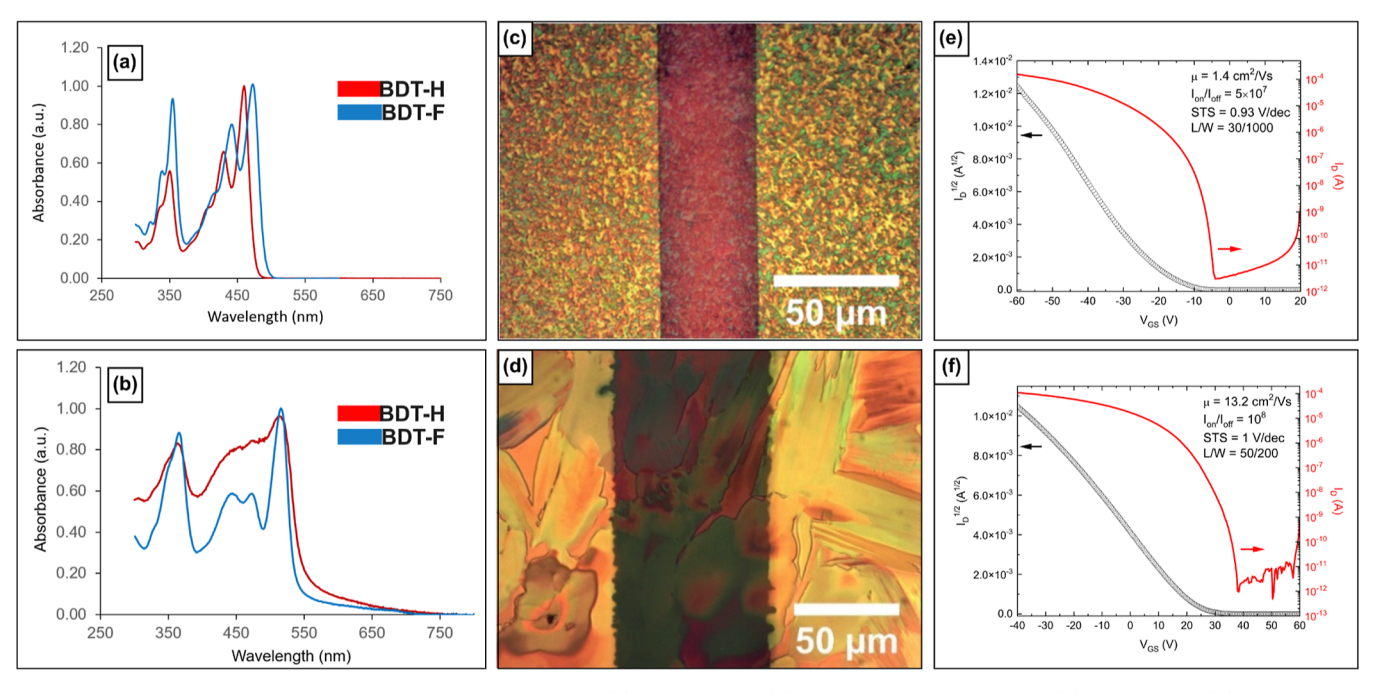


Figure 1. UV—vis absorption spectra of BDT-H and BDT-F for (a) thin film and (b) solution, optical images for (c) BDT-H and (d) BDT-F films deposited over the OFET contacts, and transfer curves for (e) BDT-H and (f) BDT-F OFETs.

kinetic cutoff of 520 eV, whereas the core electrons are treated with the projector augmented wave approach. ⁵⁵ The generalized gradient approximation for the exchange—correlation functional was applied, with the Perdew—Burke—Ernzerhof (PBE) ⁵⁶ formulation to ensure the highest accuracy, as we previously explored the impacts of various functionals on the accuracy of dynamics in small molecule OSCs. ⁴⁰ Dispersion energy contributions have been included using the Grimme D3 formalism. ^{57,58} Regarding electronic and ionic loops, the threshold criteria were set at 10^{-6} eV and 10^{-2} eV/Å, respectively. For Brillouin-zone integration, a $1 \times 1 \times 1$ Monkhorst—Pack k-point grid was used during the relaxation of all models. The same computational setup was used for the phonon calculations.

Our group previously introduced DCS-Flow, a tool that simulates the INS spectrum based on phonon mode calculations. The phonons were calculated using the supercell method implemented with phonopy. Continuing further, DCS-Flow models the INS spectrum using the energies and forces from DFT, employing the oCLIMAX tool provided by Oak Ridge National Laboratory. The INS spectra have been simulated for all considered possibilities of syn- and anti-isomers of both BDT-H and BDT-F trimer structures and compared to experimental data.

Molecular Calculations. The molecular geometries of all the calculations have been performed using the Gaussian 16 package. The B3LYP⁶³ functional with D3 dispersion to correction, combining the 6-31G(d)⁶⁵ basis set, is used for all the calculations in the gas phase. To obtain a benchmark for the dihedral angle distortion in the backbones of anti- and synisomers of BDT-H and BDT-F trimers, as well as for the structures in which sulfur atoms have been replaced with selenium atoms, we employed the following methods: two standard DFT functionals (PBE⁵⁶ and M06-L⁶⁶) and five hybrid functionals (B3LYP, HSE06, HSE06, MO6, MO6-2X, and M06-HF⁶⁹). The frontier molecular orbitals were calculated by using dimers extracted from the molecular crystals.

RESULTS AND DISCUSSION

Optical and Electrical Properties. Figure 1a shows the UV/vis spectra of the two BDT trimers dissolved in toluene. Several differences in the spectra are of note and help to understand the dissolved state structure. Both molecules show a higher ratio of 0-0 to 0-1 vibronic coupling, indicating negligible structural changes between the ground and excited state. In other words, even in solution, the BDT end groups are largely planar with the central BDT. The peak widths are narrower for the BDT-H trimer, indicating greater similarity for the molecular environments than for the BDT-F trimer. We speculate that the side chains interact more strongly with the BDT-F, causing greater constraints on the configurations of the BDT chromophores. This assignment is validated by clear Hbond interactions between the side chains and fluorine in vacuum phase structural minimizations; see Figure S10. Also, the BDT-F trimer is slightly red-shifted, possibly indicating greater planarization of the backbone in the solution. Both film spectra in Figure 1b show a significant red-shift of ~70-80 nm that could indicate (1) that the film configuration is significantly more planar in both samples than the dissolved configuration and/or (2) intermolecular delocalization of the ground state wave function across multiple molecules. The BDT-F still shows a regular vibronic progression, which is a sign that the backbone configuration is fairly uniform, but there is also a broader peak centered at 430 nm indicative of amorphous molecules or an amorphous phase. In contrast, the BDT-H spectrum is very broadened with no vibronic progression, indicating a wide variety of molecular configurations and/or a large percentage of disordered/amorphous molecules.

Figure 1c,d shows microscopy images of the BDT-H and BDT-F trimer films, respectively, on the OFET bottom contacts. The BDT-H trimer sample has very small domains that are random in shape (edges not straight and uneven corners), which is consistent with the film UV/vis spectrum showing a variety of molecular structures. In comparison, the

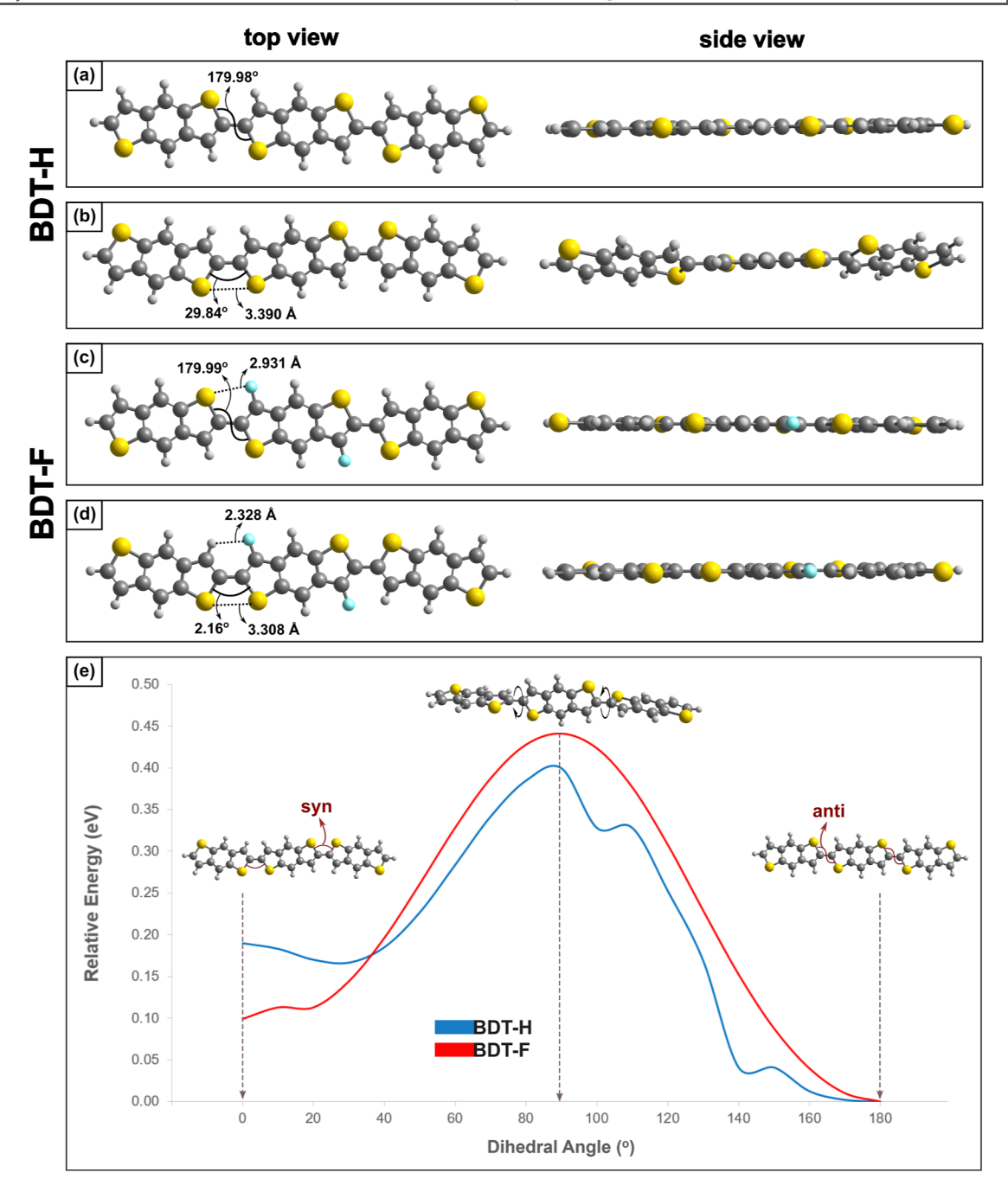


Figure 2. Dihedral angle between BDT units in the backbone of anti- and syn-isomers of (a,b) BDT-H and (c,d) BDT-F structures by considering H atoms as a side chain. (e) DFT-calculated torsion potentials of BDT-H (blue) and BDT-F (red).

BDT-F trimer shows large (1 s to 10 s of μ m) domains with straight edges and angular corners, consistent with a highly crystalline sample. Figure 1e,f shows the transfer curves of optimized OFET devices for BDT-H and BDT-F trimers, respectively, while in Figures S6 and S7, we include the corresponding output curves.

As in our original study, 30 the field-effect mobilities in the BDT-H trimer were in the order of 1 cm 2 V $^{-1}$ s $^{-1}$. The high electrical performance is accompanied by exceptional operational stability under high, constant bias conditions. This is evidenced by the minimal threshold voltage shift, which remain below 1 V, even after extensive testing in an ambient environment. Remarkably, the mobility values in the BDT-F trimer exceeded $10 \text{ cm}^2 \text{ V}^{-1} \text{ s}^{-1}$, with the device included in

Figure 1f displaying a value of 13 cm 2 V $^{-1}$ s $^{-1}$. Additionally, these OFETs are also characterized by high on/off ratios (10^7 to 10^8) and sharp turn on, with subthreshold swings around 1 V dec $^{-1}$. The order of magnitude enhancement in the charge carrier mobility in the fluorinated trimer is partially due to the presence of the larger grains, but additional factors play a role, as we describe below.

Based on detailed sulfur occupancy analysis in the crystallographic data for the BDT-H trimer, we were surprised to find substantial disorder around the single bonds that link the BDT units together. In crystals of oligothiophene systems, the anti-configuration is strongly preferred. However, there have been instances in longer oligothiophenes where synorientations were found, and the prevalence of syn-

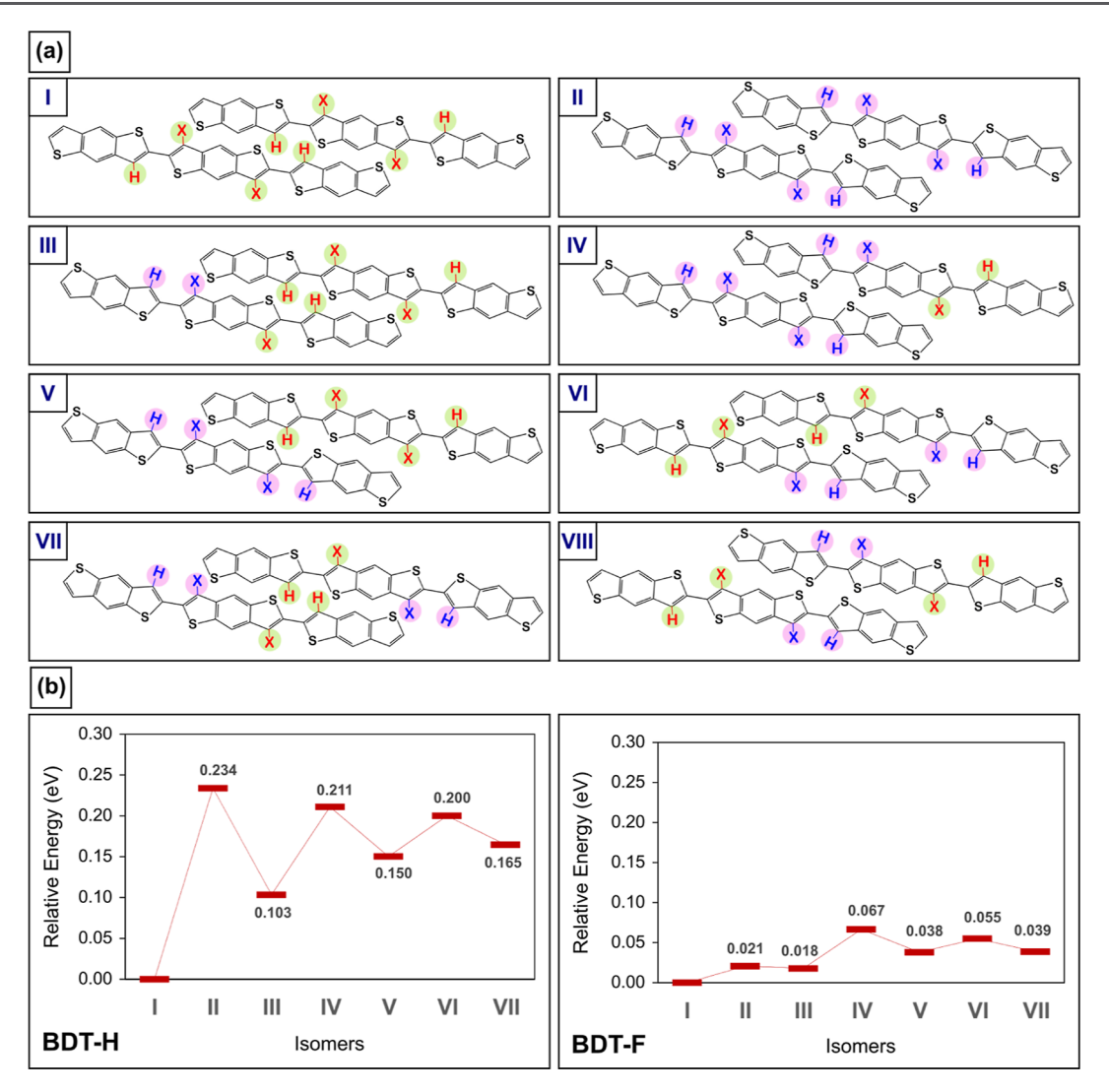


Figure 3. (a) Considered anti- and syn-isomers (I–VIII, X = H, or F) and (b) their relative energies for BDT-H (X = H, left) and BDT-F (X = F, right) in the unit cell of the periodic system. To simplify showing the isomers, the silylethyne side chain groups are removed.

contamination also appears to be related to the nature of the solubilizing groups along the chromophore backbone.³⁰ In the BDT trimers studied here, they showed as much as a 56% incidence of syn-isomer in the crystal (e.g., Figure 3, isomers VI and VII, or in some cases, both BDT linkages likely adopt the syn-configuration, isomer II or V).

Taking all of the measured data together, we can clearly state that the selective fluorination of the BDT backbone increases the formation of crystals with long-range order, generates a uniform film vibronic structure that is indicative of an ordered backbone, and produces FETs with >10× higher $\mu_{\rm h}$ compared to the BDT-H trimer. The measurement of $\mu_{\rm h}=13~{\rm cm}^2~{\rm V}^{-1}~{\rm s}^{-1}$ in the best devices is one of the highest reported $\mu_{\rm h}$'s ever reported. This sample is, therefore, of high interest. It is of paramount importance to understand exactly why selective fluorine substitution makes the BDT-F trimer so much better than the BDT-H trimer.

Backbone and Intramolecular Structure. Intramolecular noncovalent interactions, such as heteroatom interactions and hydrogen bonds, play a significant role in the crystal engineering of OSCs and their properties. ^{70–72} While electrostatic interactions between sulfur and neighboring heteroatoms, like fluorine atoms within the same molecule or polymer

chain, ^{73,74} are crucial, hydrogen bonding within conjugated polymers can exhibit even greater strength. ^{75–77} For the BDT-H trimer, there are no hydrogen bonds or F···S attractive interactions, only S···S repulsion between neighboring BDT rings (Scheme 1c). By comparison, in the anti-conformer of the BDT-F trimer, we observe S···F attractive interactions, while in the syn-configuration, we observe H-bond (H···F) attraction and S···S repulsion between neighboring BDTs (Scheme 1d).

To assess and better understand the intramolecular interaction within the backbone without interference from the side chains, we replaced the side chains with hydrogen atoms. Two molecules with both syn- and anti-conformers in the backbone of the BDT trimers were considered. Figure 2a—d shows the optimized structures of both the BDT-H and BDT-F trimer structures. Surprisingly, both two isomers of the BDT-F trimer are almost planar, while in BDT-H, the anti-conformer is planar, but the syn-orientation still exhibits a dihedral angle of approximately 30°. These observations reveal that the presence of S···S (3.390 Å) noncovalent repulsion in the syn-conformer of the BDT-H trimer is important and that it prevents the molecule from assuming a planar and well delocalized geometry. In the case of the BDT-F trimer, the

hydrogen bond has a remarkable planarizing effect. It can effectively overcome the dihedral angle distortion caused by the S···S repulsion, causing the syn-conformer to become nearly planar. To examine the strength of hydrogen bonds in overcoming dihedral angle distortion, we examined both BDT-H and BDT-F trimers in a syn- and anti-configurations, wherein sulfur atoms were substituted with the heavier isovalent element, selenium (Se). The results reveal that in the BDT-H syn-structure, the dihedral angle exceeds 30°, whereas, with fluorination, the syn-dihedral angle reduces to 12°; see Supporting Information, Figure S11. In conclusion, two potential strategies can be considered to overcome this significant torsion angle: first, by minimizing the S···S repulsion and going to an anti-orientation; second, by introducing a stronger hydrogen bond on the opposite side through the replacement of a H atom with a F atom (Scheme 1b).

To investigate the energetic cost associated with rotating the terminal BDT units in both BDT-H and BDT-F trimer structures, as well as to examine the impact of H bonding on this process, the torsion potentials were calculated by varying the dihedral angle and calculating the configuration energy. The results are presented in Figure 2e. Upon comparing the relative energies of BDT-H and BDT-F trimers, it becomes evident that the presence of a H bond in the syn-configuration of BDT-F enhances their stability within the range of 0-40 degrees of dihedral distortion, in contrast to BDT-H structures. However, as dihedral distortion increases, leading to the disappearance of the hydrogen bond, the relative energies of the BDT-H trimer become lower than those of the BDT-F trimer. It can be concluded that flipping terminal BDT units in BDT-H is easier than in BDT-F and that planar synconfigurations are relatively stable in BDT-F. Finally, for both molecules, the difference between anti- and synconfigurations is less than kT. So, while anti-configurations should be more common, we expect ~40% syn-configurations based on stability differences.

In order to assess the reliability of the method in predicting intramolecular interactions and dihedral angle distortions in the backbone of BDT trimers and in structures in which S atoms are replaced with Se atoms, we conducted benchmark tests using various pure and hybrid functional methods. The results are presented in Table S2. Both pure and hybrid functionals give the same result for all anti structures: the dihedral angle is 180° without any distortion. Two hybrid functionals with 22 and 100% of exact exchange (ω B97X-D and M06-HF, respectively) show the maximum distortion, with angles of 35 and 40°, while the pure DFT functional has the minimum dihedral angle (13-22°) in the syn-isomer of BDT-H. In the syn BDT-F cases, the ω B97X-D and M06-HF functionals still exhibit distortion by 19 and 24°, respectively, while the remaining functionals show the planar structures. By replacing the S atom with Se and increasing Se...Se repulsion, we observe the same trends, although some changes in distortion can be observed.

We next explore the dihedral angle disorder as a feature of intramolecular interactions within the backbone of BDT trimers in the presence of the side chains. We considered individual molecules in the gas phase compared with the geometry of the molecule in the periodic system. The results indicate that the distortion of both syn- and anti-orientations for both the BDT-H and BDT-F molecules is significantly larger, up to 28°, compared to the dihedral angle observed in the crystalline structure, which was less than 8° (Supporting

Information, Figure S10). In the free molecule, the interactions between the side chain and backbone of the BDTs cause this distortion, which is not expected in the crystal.

Crystalline Configurations. Most simulation research on OSCs has focused on studying individual molecules, dimers, or clusters of molecules in the gas phase.^{9,78} Researchers have found that structures with the ability to isomerize, such as antiand syn-conformers, tend to favor the anti-isomer. 78,79 This type of simulation determines the minimized structure or structure that is most likely to form. However, if the difference between the minimized structure and other configurations has energetic differences that are less than kT, then a variety of isomers will form. To address this issue, we model all eight isomers (Figure 3a) for unit cells of two BDT trimers. These include two highly symmetric structures with all BDT units in anti (I) or syn (II) positions, as well as configurations where one BDT unit in one of the two molecules is rotated (III and IV). Additionally, we examined structures with two syn- and anti-conformers in the BDT trimer (V to VIII). Note that isomers VII and VIII are identical when the unit cell is repeated in the periodic system, as shown in Supporting Information, Figure S9, thus VIII is not labeled in Figure 3b.

The results for the minimization of both BDT-H and BDT-F structures are summarized graphically in Figure 3b, where the relative energy of each isomer is referenced to the most stable one. For the BDT-H trimer, the anti/anti (I) and syn/syn (II) isomers are the most and least stable, respectively, with a 0.23 eV difference. Flipping one BDT unit in I costs 0.1 eV to obtain isomer III, while the same rotation in isomer II, resulting in isomer IV, costs about 0.02 eV. In the remaining anti/syn isomers (V-VII), their stabilities are almost equivalent, less than 0.2 eV. In the case of fluorination, compared to BDT-H, the variation range of relative energy is smaller, and the relative energies are less than 0.07 eV, 3b. Similar to BDT-H, isomer I is the most favorable, while isomer II is only 0.02 eV less stable. Isomer IV is the least favorable, and the remaining isomers are almost equivalent. The presence of H-bonding in isomer II has decreased the relative energy differences between the isomers compared to the nonfluoridated one. Comparing the energetic differences between BDT-F and BDT-H, we would predict much more isomerization within the crystal structure for BDT-F because the relative stability differences are smaller. Since greater isomerization is usually associated with a higher trap density, BDT-F has a significantly higher μ_h than BDT-H. This suggests that the BDT-F can have high μ_h even with significant isomerization within the same crystal because each individual BDT-F site is planar and has similar ground state energy.

The structural data for all isomers are summarized in Tables S3—S6. Since the BDT-F trimer is planar in both anti- and synconfigurations, it is worth asking whether the S···F in the anticonfiguration does a better job of planarizing the backbone than the H···F bond in the syn-configuration. To simplify our comparison, we consider the summation of both dihedral angles in each molecule, Tables S4 and S5. The dihedral angles for the planar syn- and anti-isomers are 0 and 180°, respectively. To facilitate the summation, we assume the dihedral angle of the anti-isomer to be 0° by reducing it from 180°. Upon comparing the relative energies of dimers of BDT-F trimers, we can conclude that the F···H interaction has more effect over the S···F contact. The bond lengths of the hydrogen bonds fall within the range of 2.39 –2.46 Å (see Table S5), aligning with the reported intra- and intermolecular H bonding

distances observed in crystal engineering studies (up to 2.9 Å). 76 In summary, the BDT-H isomers exhibit dihedral angles for both anti- and syn-conformers in the range of $2-6^{\circ}$, while for the BDT-F isomers, the dihedral angles are in the range of $1-4^{\circ}$, much reduced compared to the BDT-H isomers, see Tables S4 and S5. The consequence on long-range ordering is significant. As seen in Figure 1c, the BDT-H trimer exhibits very small crystallites and reduced $\mu_{\rm h}$ compared to BDT-F trimers, with long-range ordering in crystallites of up to $10~\mu_{\rm h}$ and $>10\times$ greater $\mu_{\rm h}$. The longer range ordering in BDT-F trimers is clearly better for high $\mu_{\rm h}$; however, the large variety of isomers in the crystal predicts a high energetic disorder within the crystallites. We perform a more detailed analysis of the intermolecular structure in the next section.

Model Validation to INS Data. In this section, we discuss the INS results obtained for both the BDT-H and BDT-F trimers. INS measures the motions of all of the nuclei with equal scattering signals coming from atoms in crystalline and amorphous domains. This means that the INS spectrum is a weighted density of motion states. Since the atomic environment around an atom affects its dynamics, it is possible to quantitatively divide an INS spectrum into populations that represent molecules in differing geometries. The INS spectrum from VISION covers phonon modes over three orders of energy, corresponding to physical motions as fast as a C–H stretch (~3500 cm⁻¹) down to collective intermolecular phonons involving 100s of atoms over multiple nm in the (10–100 cm⁻¹) range.

Figure 4 (black) shows the measured INS spectrum in energy ranges corresponding to intermolecular phonons (5-350 cm⁻¹) and the C-H wag and bend modes for sp²hybridized orbitals (600-1000 cm⁻¹). Below the measured spectra are simulated INS spectra of each different configuration, as shown in Figure 4. In the BDT-F simulation, there is a near quantitative agreement over 3 orders of magnitude in energy between the experimental and simulated results, validating our computational methods. 54,59 In several regions of the spectrum, for example, the doublet at 250 cm⁻¹ and the four small peaks between 725 and 810 cm⁻¹, the peak position changes because the protons on the pendant BDT experience shifts in their vibrational frequency due to differences in the molecular environment in the different isomers. At the bottom in gray, Figure 4, is a weighted sum of spectra with the percentage weight of each spectrum determined by the Boltzmann population from the energies displayed in Figure 3b. At about 250 cm⁻¹, isomers II and IV with mostly syn show a clear doublet, while isomers I, III, V, and VII with at least 1/2 anti-configurations show a broadened singlet. The measured and sum spectra depict a close doublet representing a variety of configurations in the same crystal. Also, at 725-810 cm⁻¹, all anti-isomer I shows two broad peaks, but most of the isomers with syn-configurations show two doublets. The sum spectrum shows two doublets, but the measured spectrum has only two broad peaks. In this case, the result is less clear because the measured large peak at 735 cm⁻¹ red-shifted 20 to 715 cm⁻¹ in the simulated spectrum. It can be safely concluded from these spectra that multiple different isomers of syn/anti-configurations are incorporated into the same crystal in BDT-F. The highly planar structure of both syn- and anti-bonds enables significant structural variation within the same crystal.

As discussed from the crystalite size and UV/vis spectrum, the BDT-H trimer exhibits greater structural anisotropy than

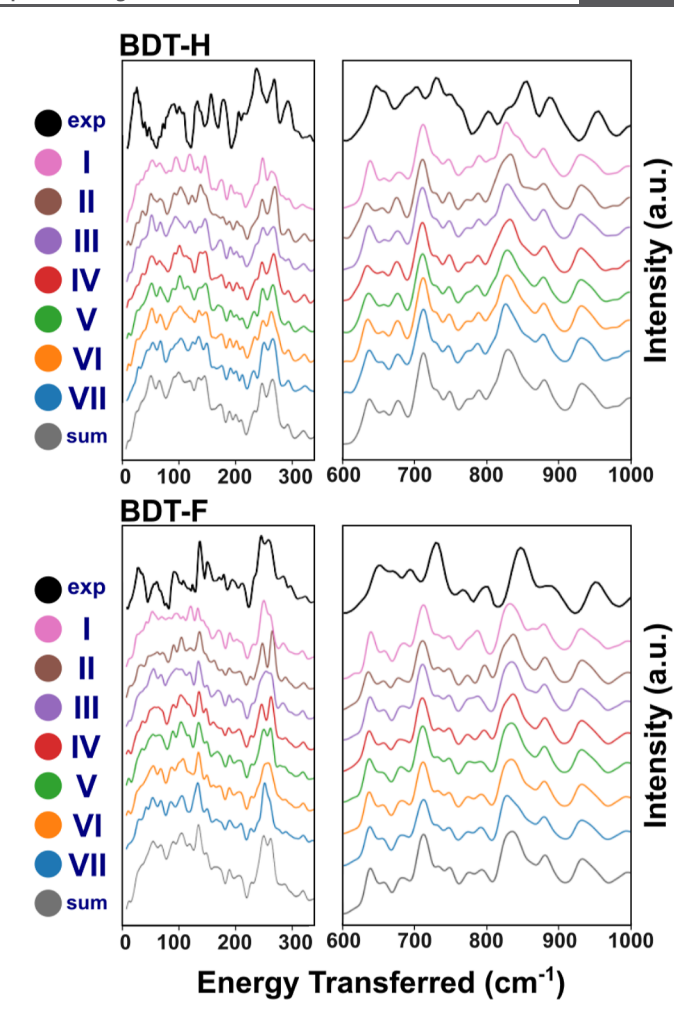


Figure 4. Experimental and simulated INS spectrum for I–VII isomers of BDT-H and BDT-F structures are shown in Figure 3a. Left and right show the INS of the entire energy range and a close-up of the spectra.

BDT-F. This increased complexity is shown by a larger number of peaks compared with the BDT-F trimer. The increased complexity in the BDT-H trimer comes from the reduced crystallinity, meaning that the protons in the BDT-H trimer sample experience a greater variety of molecular environments. The relatively poor quantitative fit to the simulated data is due to the fact that a majority of the BDT-H molecules are not incorporated into extended crystals. Instead, the large portions of this sample have molecules with dihedral angles of $\sim 30^{\circ}$ that cannot be included into organized crystals.

CONCLUSIONS

Through the fluorination of BDT-H (Scheme 1b), a new OSC has been reported, exhibiting hole mobility as high as $13.2~{\rm cm}^2~{\rm V}^{-1}~{\rm s}^{-1}$. We employed a comparative study using both vacuum DFT, including two pure DFT functionals and seven different hybrid functionals, as well as plane wave DFT + U, including dispersion contributions, to gain a better understanding of the role of fluorine atoms in guiding the design of new generations of OSC materials. We find that single molecule simulations reveal biased molecular forces but fail to capture the planarization of dihedral bonds due to the nearest neighbors in a crystal. The results can be summarized with the following points:

- Although the through space interaction of fluorine with sulfur is the main contributor to dihedral planarization, H-bonding formed through selective fluorination is critical. Through space, S···F and H···F interactions along the backbone stabilize planarization while S···S interactions in syn-configurations rotate the dihedral bond out-of-plane. Simulations of each dimer crystal configuration revealed a direct and significant effect: the dihedral bonds in BDT-F are either near 0° or 180° for all isomers.
- A crystal structure containing a mixture of several configurations could have significant mobility, while the dihedral disorder is mitigated by configurations that are energetically very similar. Also, different isomers of the same crystal stack into the same crystal, and the relative difference between isomers for BDT-F is significantly lower than for BDT-H, meaning that a crystal of BDT-F is composed of multiple different structures. This result is directly opposed to the typical view that only a perfectly repeating structure can have high charge delocalization and high μh. The comparison between BDT-F and BDT-H shows that multiple crystalline isomers can support high μh if all of the isomers are planar and have small relative energetic differences between their ground state structures.

INS spectroscopy was used to measure the vibrational spectra of the BDT-H and BDT-F samples. A near quantitative match between the spectra and simulations was used to validate the structural assignments from DFT. Several spectral regions in the INS spectrum could be isolated that fingerprint syn- and anti-BDT dihedral configurations. Notably, both the data and simulations agree that it is essential to consider all combinations of syn- and anti-conformers and that multiple isomers can be accommodated into high $\mu_{\rm h}$ crystals. We speculate that the oligomeric structure accommodates higher structural disorder without losing delocalization based on longrange order.

ASSOCIATED CONTENT

Supporting Information

The Supporting Information is available free of charge at https://pubs.acs.org/doi/10.1021/acs.chemmater.4c00640.

Details on the synthesis of BDT-F, output curves, simulated INS spectra, and structural data (PDF)

AUTHOR INFORMATION

Corresponding Author

Adam J. Moulé — Department of Chemical Engineering, University of California Davis, Davis, California 9S616, United States; o orcid.org/0000-0003-1354-3517; Email: amoule@ucdavis.edu

Authors

Farahnaz Maleki — Department of Chemical Engineering, University of California Davis, Davis, California 95616, United States; o orcid.org/0000-0002-5747-1319

Karl J. Thorley — Department of Chemistry, University of Kentucky, Lexington, Kentucky 40506, United States; orcid.org/0000-0003-0665-3363

Hamna F. Iqbal – Department of Physics and Center for Functional Materials, Wake Forest University, Winston-Salem, North Carolina 27109, United States

- Daniel Vong Department of Materials Science and Engineering, University of California Davis, Davis, California 95616, United States; orcid.org/0000-0003-1348-5302
- Toulik Maitra Department of Chemical Engineering, University of California Davis, Davis, California 95616, United States
- Anthony Petty Department of Chemistry, University of Kentucky, Lexington, Kentucky 40506, United States; orcid.org/0000-0002-5831-0314
- Luke L. Daemen Neutron Scattering Division, Oak Ridge National Laboratory, Oak Ridge, Tennessee 37830, United States
- Sean R. Parkin Department of Chemistry, University of Kentucky, Lexington, Kentucky 40506, United States
- Oana D. Jurchescu Department of Physics and Center for Functional Materials, Wake Forest University, Winston-Salem, North Carolina 27109, United States; orcid.org/0000-0003-2204-2909
- John E. Anthony Department of Chemistry, University of Kentucky, Lexington, Kentucky 40506, United States; orcid.org/0000-0002-8972-1888

Complete contact information is available at: https://pubs.acs.org/10.1021/acs.chemmater.4c00640

Notes

The authors declare no competing financial interest.

ACKNOWLEDGMENTS

This research was supported by the Department of Energy, Basic Energy Sciences, Award DE-SC0023123, including salary for F.M., D.V., T.M., and A.J.M. This research used resources of the National Energy Research Scientific Computing Center (NERSC), a DOE Office of Science User Facility supported by the Office of Science of the U.S. Department of Energy under contract no. DE-AC02-05CH11231. This research used resources at the Spallation Neutron Source, a DOE Office of Science User Facility operated by the Oak Ridge National Laboratory. This work was also partly supported by LLNL under contract DE-AC52-07NA27344. The NSF has supported the work at WFU under DMR awards 1627925 and 2323423 and at UK under DMR-1627428. All opinions expressed in this paper are the author's and do not necessarily reflect the policies and views of DOE, ORAU, or ORISE.

■ REFERENCES

- (1) Hains, A. W.; Liang, Z.; Woodhouse, M. A.; Gregg, B. A. Molecular semiconductors in organic photovoltaic cells. *Chem. Rev.* **2010**, *110*, 6689–6735.
- (2) Lin, Y.; Li, Y.; Zhan, X. Small molecule semiconductors for high-efficiency organic photovoltaics. *Chem. Soc. Rev.* **2012**, *41*, 4245–4272.
- (3) Wang, C.; Dong, H.; Jiang, L.; Hu, W. Organic semiconductor crystals. *Chem. Soc. Rev.* **2018**, 47, 422–500.
- (4) Hamers, R. J. Flexible electronic futures. *Nature* **2001**, 412, 489–490.
- (5) Usta, H.; Facchetti, A. Flexible Carbon-Based Electronics; Wiley, 2018; pp 13-49.
- (6) Liu, K.; Ouyang, B.; Guo, X.; Guo, Y.; Liu, Y. Advances in flexible organic field-effect transistors and their applications for flexible electronics. *npj Flexible Electron.* **2022**, *6*, 1.
- (7) Das, B.; Dolai, M.; Ghosh, A.; Dhara, A.; Mahapatra, A. D.; Chattopadhyay, D.; Mabhai, S.; Jana, A.; Dey, S.; Misra, A. A biocompatible pyridine—pyrazole hydrazide based compartmental

- receptor for Al 3+ sensing and its application in cell imaging. *Anal. Methods* **2021**, *13*, 4266–4279.
- (8) Zeidell, A. M.; Ren, T.; Filston, D. S.; Iqbal, H. F.; Holland, E.; Bourland, J. D.; Anthony, J. E.; Jurchescu, O. D. Organic field-effect transistors as flexible, tissue-equivalent radiation dosimeters in medical applications. *Advanced Science* **2020**, *7*, 2001522.
- (9) Bhat, V.; Callaway, C. P.; Risko, C. Computational approaches for organic semiconductors: from chemical and physical understanding to predicting new materials. *Chem. Rev.* **2023**, *123*, 7498–7547.
- (10) Troisi, A. Charge transport in high mobility molecular semiconductors: classical models and new theories. *Chem. Soc. Rev.* **2011**, *40*, 2347–2358.
- (11) Schweicher, G.; d'Avino, G.; Ruggiero, M. T.; Harkin, D. J.; Broch, K.; Venkateshvaran, D.; Liu, G.; Richard, A.; Ruzié, C.; Armstrong, J.; Kennedy, A. R.; et al. Chasing the "killer" phonon mode for the rational design of low-disorder, high-mobility molecular semiconductors. *Adv. Mater.* **2019**, *31*, 1902407.
- (12) Schweicher, G.; Garbay, G.; Jouclas, R.; Vibert, F.; Devaux, F.; Geerts, Y. H. Molecular semiconductors for logic operations: deadend or bright future? *Adv. Mater.* **2020**, *32*, 1905909.
- (13) Ortiz, R. P.; Casado, J.; Hernández, V.; Navarrete, J. L.; Letizia, J. A.; Ratner, M. A.; Facchetti, A.; Marks, T. J. Thiophene—Diazine Molecular Semiconductors: Synthesis, Structural, Electrochemical, Optical, and Electronic Structural Properties; Implementation in Organic Field-Effect Transistors. *Chem.—Eur. J.* 2009, *15*, 5023—5039.
- (14) Huang, H.; Yang, L.; Facchetti, A.; Marks, T. J. Organic and polymeric semiconductors enhanced by noncovalent conformational locks. *Chem. Rev.* **2017**, *117*, 10291–10318.
- (15) Mishra, A.; Bäuerle, P. Small molecule organic semiconductors on the move: promises for future solar energy technology. *Angew. Chem., Int. Ed.* **2012**, *51*, 2020–2067.
- (16) Freudenberg, J.; Jänsch, D.; Hinkel, F.; Bunz, U. H. Immobilization strategies for organic semiconducting conjugated polymers. *Chem. Rev.* **2018**, *118*, 5598–5689.
- (17) Ruhle, V.; Kirkpatrick, J.; Andrienko, D. A multiscale description of charge transport in conjugated oligomers. *J. Chem. Phys.* **2010**, *132*, 134103.
- (18) Huang, C.-F.; Wu, S.-L.; Huang, Y.-F.; Chen, Y.-C.; Chang, S.-T.; Wu, T.-Y.; Wu, K.-Y.; Chuang, W.-T.; Wang, C.-L. Packing Principles for Donor—Acceptor Oligomers from Analysis of Single Crystals. *Chem. Mater.* **2016**, *28*, 5175–5190.
- (19) Zade, S. S.; Zamoshchik, N.; Bendikov, M. From short conjugated oligomers to conjugated polymers. Lessons from studies on long conjugated oligomers. *Acc. Chem. Res.* **2011**, *44*, 14–24.
- (20) Nematiaram, T.; Troisi, A. Strategies to reduce the dynamic disorder in molecular semiconductors. *Mater. Horiz.* **2020**, *7*, 2922–2928
- (21) Wang, Q.; Böckmann, S.; Günther, F.; Streiter, M.; Zerson, M.; Scaccabarozzi, A. D.; Tan, W. L.; Komber, H.; Deibel, C.; Magerle, R.; Gemming, S.; et al. Hydrogen bonds control single-chain conformation, crystallinity, and electron transport in isoelectronic diketopyrrolopyrrole copolymers. *Chem. Mater.* **2021**, *33*, 2635–2645.
- (22) Lehnherr, D.; Waterloo, A. R.; Goetz, K. P.; Payne, M. M.; Hampel, F.; Anthony, J. E.; Jurchescu, O. D.; Tykwinski, R. R. Isomerically pure syn-anthradithiophenes: synthesis, properties, and FET performance. *Org. Lett.* **2012**, *14*, 3660–3663.
- (23) Diemer, P. J.; Hayes, J.; Welchman, E.; Hallani, R.; Pookpanratana, S. J.; Hacker, C. A.; Richter, C. A.; Anthony, J. E.; Thonhauser, T.; Jurchescu, O. D. The influence of isomer purity on trap states and performance of organic thin-film transistors. *Adv. Electron. Mater.* **2017**, *3*, 1600294.
- (24) Huang, C.-W.; You, X.; Diemer, P. J.; Petty, A. J.; Anthony, J. E.; Jurchescu, O. D.; Atkin, J. M. Micro-Raman imaging of isomeric segregation in small-molecule organic semiconductors. *Commun. Chem.* **2019**, *2*, 22.
- (25) Iqbal, H. F.; Holland, E. K.; Anthony, J. E.; Jurchescu, O. D. Real-time monitoring of trap dynamics reveals the electronic states

- that limit charge transport in crystalline organic semiconductors. *Mater. Horiz.* **2020**, *7*, 2390–2398.
- (26) Hallani, R. K.; Thorley, K. J.; Mei, Y.; Parkin, S. R.; Jurchescu, O. D.; Anthony, J. E. Structural and electronic properties of crystalline, isomerically pure anthradithiophene derivatives. *Adv. Funct. Mater.* **2016**, *26*, 2341–2348.
- (27) Mamada, M.; Minamiki, T.; Katagiri, H.; Tokito, S. Synthesis Physical properties, and field-effect mobility of isomerically pure syn-/anti-anthradithiophene derivatives. *Org. Lett.* **2012**, *14*, 4062–4065.
- (28) Mamada, M.; Katagiri, H.; Mizukami, M.; Honda, K.; Minamiki, T.; Teraoka, R.; Uemura, T.; Tokito, S. Syn-/anti-anthradithiophene derivative isomer effects on semiconducting properties. ACS Appl. Mater. Interfaces 2013, 5, 9670–9677.
- (29) Fratini, S.; Nikolka, M.; Salleo, A.; Schweicher, G.; Sirringhaus, H. Charge transport in high-mobility conjugated polymers and molecular semiconductors. *Nat. Mater.* **2020**, *19*, 491–502.
- (30) Petty, A. J.; Ai, Q.; Sorli, J. C.; Haneef, H. F.; Purdum, G. E.; Boehm, A.; Granger, D. B.; Gu, K.; Rubinger, C. P. L.; Parkin, S. R.; Graham, K. R.; et al. Computationally aided design of a high-performance organic semiconductor: the development of a universal crystal engineering core. *Chem. Sci.* **2019**, *10*, 10543–10549.
- (31) Wang, Y.; Tan, A. T.-R.; Mori, T.; Michinobu, T. Inversion of charge carrier polarity and boosting the mobility of organic semiconducting polymers based on benzobisthiadiazole derivatives by fluorination. *J. Mater. Chem. C* **2018**, *6*, 3593–3603.
- (32) Chen, H.; Ling, M.; Mo, X.; Shi, M.; Wang, M.; Bao, Z. Air stable n-channel organic semiconductors for thin film transistors based on fluorinated derivatives of perylene diimides. *Chem. Mater.* **2007**, *19*, 816–824.
- (33) Cheng, Y.; Qi, Y.; Tang, Y.; Zheng, C.; Wan, Y.; Huang, W.; Chen, R. Controlling intramolecular conformation through non-bonding interaction for soft-conjugated materials: molecular design and optoelectronic properties. *J. Phys. Chem. Lett.* **2016**, *7*, 3609–3615.
- (34) Haque, A.; Alenezi, K. M.; Khan, M. S.; Wong, W.-Y.; Raithby, P. R. Non-covalent interactions (NCIs) in π -conjugated functional materials: advances and perspectives. *Chem. Soc. Rev.* **2023**, *52*, 454–472.
- (35) Ji, X.; Cheng, H.-W.; Schuster, N. J.; LeCroy, G. S.; Zhang, S.; Wu, Y.; Michalek, L.; Nguyen, B.-N. T.; Chiong, J. A.; Schrock, M.; Tomo, Y.; et al. Tuning the Mobility of Indacenodithiophene-Based Conjugated Polymers via Coplanar Backbone Engineering. *Chem. Mater.* **2023**, *36*, 256–265.
- (36) Saito, M.; Fukuhara, T.; Kamimura, S.; Ichikawa, H.; Yoshida, H.; Koganezawa, T.; Ie, Y.; Tamai, Y.; Kim, H. D.; Ohkita, H.; Osaka, I. Impact of Noncovalent Sulfur—Fluorine Interaction Position on Properties, Structures, and Photovoltaic Performance in Naphthobisthiadiazole-Based Semiconducting Polymers. *Adv. Energy Mater.* **2020**, *10*, 1903278.
- (37) Zhu, C.; Fang, L. Locking the Coplanar Conformation of π -Conjugated Molecules and Macromolecules Using Dynamic Noncovalent Bonds. *Macromol. Rapid Commun.* **2018**, *39*, 1700241.
- (38) Illig, S.; Eggeman, A. S.; Troisi, A.; Jiang, L.; Warwick, C.; Nikolka, M.; Schweicher, G.; Yeates, S. G.; Henri Geerts, Y.; Anthony, J. E.; Sirringhaus, H. Reducing dynamic disorder in small-molecule organic semiconductors by suppressing large-amplitude thermal motions. *Nat. Commun.* **2016**, *7*, 10736.
- (39) Facchetti, A.; Yoon, M.-H.; Stern, C. L.; Hutchison, G. R.; Ratner, M. A.; Marks, T. J. Building blocks for N-type molecular and polymeric electronics. perfluoroalkyl-versus alkyl-functionalized oligothiophenes (NTs; n= 2- 6). systematic synthesis, spectroscopy, electrochemistry, and solid-state organization. *J. Am. Chem. Soc.* **2004**, *126*, 13480–13501.
- (40) Harrelson, T. F.; Dantanarayana, V.; Xie, X.; Koshnick, C.; Nai, D.; Fair, R.; Nuñez, S. A.; Thomas, A. K.; Murrey, T. L.; Hickner, M. A.; Grey, J. K.; et al. Direct probe of the nuclear modes limiting charge mobility in molecular semiconductors. *Mater. Horiz.* **2019**, *6*, 182–191.

- (41) Vong, D.; Nematiaram, T.; Dettmann, M. A.; Murrey, T. L.; Cavalcante, L. S.; Gurses, S. M.; Radhakrishnan, D.; Daemen, L. L.; Anthony, J. E.; Koski, K. J.; Kronawitter, C. X.; et al. Quantitative hole mobility simulation and validation in substituted acenes. *J. Phys. Chem. Lett.* **2022**, *13*, 5530–5537.
- (42) Hudson, B. S. Vibrational spectroscopy using inelastic neutron scattering: Overview and outlook. *Vib. Spectrosc.* **2006**, *42*, 25–32.
- (43) Cavalcante, L. S.; Dettmann, M. A.; Sours, T.; Yang, D.; Daemen, L. L.; Gates, B. C.; Kulkarni, A. R.; Moulé, A. J. Elucidating correlated defects in metal organic frameworks using theory-guided inelastic neutron scattering spectroscopy. *Mater. Horiz.* **2023**, *10*, 187–196.
- (44) Harrelson, T. F.; Cheng, Y. Q.; Li, J.; Jacobs, I. E.; Ramirez-Cuesta, A. J.; Faller, R.; Moulé, A. J. Identifying atomic scale structure in undoped/doped semicrystalline P3HT using inelastic neutron scattering. *Macromolecules* **2017**, *50*, 2424–2435.
- (45) Fratini, S.; Mayou, D.; Ciuchi, S. The transient localization scenario for charge transport in crystalline organic materials. *Adv. Funct. Mater.* **2016**, 26, 2292–2315.
- (46) Dettmann, M. A.; Cavalcante, L. S. R.; Magdaleno, C. A.; Moulé, A. J. Catching the Killer: Dynamic Disorder Design Rules for Small-Molecule Organic Semiconductors. *Adv. Funct. Mater.* **2023**, *33*, 2213370.
- (47) Son, H. J.; Wang, W.; Xu, T.; Liang, Y.; Wu, Y.; Li, G.; Yu, L. Synthesis of fluorinated polythienothiophene-co-benzodithiophenes and effect of fluorination on the photovoltaic properties. *J. Am. Chem. Soc.* **2011**, *133*, 1885–1894.
- (48) Iqbal, H.; Ai, Q.; Thorley, K.; Chen, H.; McCulloch, I.; Risko, C.; Anthony, J.; Jurchescu, O. Suppressing bias stress degradation in high performance solution processed organic transistors operating in air. *Nat. Commun.* **2021**, *12*, 2352.
- (49) Lamport, Z. A.; Haneef, H. F.; Anand, S.; Waldrip, M.; Jurchescu, O. D. Tutorial: Organic field-effect transistors: Materials, structure and operation. *J. Appl. Phys.* **2018**, *124*, 071101.
- (50) Frisch, M. J.; et al. *Gaussian* 16. Revision A.01; Gaussian Inc: Wallingford CT, 2016.
- (51) Kresse, G.; Hafner, J. Ab. initio molecular dynamics for liquid metals. *Phys. Rev. B* **1993**, *47*, 558–561.
- (52) Kresse, G.; Furthmüller, J. Efficiency of ab-initio total energy calculations for metals and semiconductors using a plane-wave basis set. *Comput. Mater. Sci.* **1996**, *6*, 15–50.
- (53) Kresse, G.; Furthmüller, J. Efficient iterative schemes for ab initio total-energy calculations using a plane-wave basis set. *Phys. Rev.* B **1996**, *54*, 11169–11186.
- (54) Dettmann, M. A.; Cavalcante, L. S.; Magdaleno, C.; Masalkovaitè, K.; Vong, D.; Dull, J. T.; Rand, B. P.; Daemen, L. L.; Goldman, N.; Faller, R.; Moulé, A. J. Comparing the expense and accuracy of methods to simulate atomic vibrations in rubrene. *J. Chem. Theory Comput.* **2021**, *17*, 7313–7320.
- (55) Kresse, G.; Joubert, D. From ultrasoft pseudopotentials to the projector augmented-wave method. *Phys. Rev. B* **1999**, *59*, 1758–1775.
- (56) Perdew, J. P.; Burke, K.; Ernzerhof, M. Generalized gradient approximation made simple. *Phys. Rev. Lett.* **1996**, *77*, 3865–3868.
- (57) Grimme, S.; Antony, J.; Ehrlich, S.; Krieg, H. A consistent and accurate ab initio parametrization of density functional dispersion correction (DFT-D) for the 94 elements H-Pu. *J. Chem. Phys.* **2010**, 132, 154104.
- (58) Grimme, S.; Ehrlich, S.; Goerigk, L. Effect of the damping function in dispersion corrected density functional theory. *J. Comput. Chem.* **2011**, 32, 1456–1465.
- (59) Cavalcante, L. S.; Daemen, L. L.; Goldman, N.; Moulé, A. J. Davis Computational Spectroscopy Workflow—From Structure to Spectra. J. Chem. Inf. Model. 2021, 61, 4486–4496.
- (60) Togo, A.; Tanaka, I. First principles phonon calculations in materials science. *Scr. Mater.* **2015**, *108*, 1–5.
- (61) Togo, A. First-principles Phonon Calculations with Phonopy and Phono3py. J. Phys. Soc. Jpn. 2023, 92, 012001.

- (62) Ramirez-Cuesta, A. J. aCLIMAX 4.0.1, the new version of the software for analyzing and interpreting INS spectra. *Comput. Phys. Commun.* **2004**, *157*, 226–238.
- (63) Becke, A. D. Density-functional thermochemistry. III. The role of exact exchange. *J. Chem. Phys.* **1993**, *98*, 5648–5652.
- (64) Grimme, S.; Antony, J.; Ehrlich, S.; Krieg, H. A consistent and accurate ab initio parametrization of density functional dispersion correction (DFT-D) for the 94 elements H-Pu. *J. Chem. Phys.* **2010**, 132, 1–19.
- (65) Hehre, W. J.; Ditchfield, R.; Pople, J. A. Self—consistent molecular orbital methods. XII. Further extensions of Gaussian—type basis sets for use in molecular orbital studies of organic molecules. *J. Chem. Phys.* **1972**, *56*, 2257–2261.
- (66) Zhao, Y.; Truhlar, D. G. A new local density functional for main-group thermochemistry, transition metal bonding, thermochemical kinetics, and noncovalent interactions. *J. Chem. Phys.* **2006**, *125*, 194101.
- (67) Heyd, J.; Scuseria, G. E.; Ernzerhof, M. Hybrid functionals based on a screened Coulomb potential. *J. Chem. Phys.* **2003**, *118*, 8207–8215.
- (68) Zhao, Y.; Truhlar, D. G. The M06 suite of density functionals for main group thermochemistry, thermochemical kinetics, noncovalent interactions, excited states, and transition elements: two new functionals and systematic testing of four M06-class functionals and 12 other functionals. *Theor. Chem. Acc.* 2008, 120, 215–241.
- (69) Zhao, Y.; Truhlar, D. G. Density functional for spectroscopy: no long-range self-interaction error, good performance for Rydberg and charge-transfer states, and better performance on average than B3LYP for ground states. *J. Phys. Chem. A* **2006**, *110*, 13126–13130.
- (70) Crouch, D. J.; Skabara, P. J.; Heeney, M.; McCulloch, I.; Coles, S. J.; Hursthouse, M. B. Hexyl-substituted oligothiophenes with a central tetrafluorophenylene unit: crystal engineering of planar structures for p-type organic semiconductors. *Chem. Commun.* **2005**, 1465–1467.
- (71) Zhang, C.; Tu, X.; Luo, Y.; Hai, Y.; Yao, X.; Xian, K.; Archie Dela Peña, T.; Li, Y.; Li, Y.; Li, M.; Ye, L.; et al. Enhanced molecular planarity for high-performance photodetectors: Effect of backbone conformation via alkyl substitution position control in dithienoquinoxaline-based conjugated polymers. *Chem. Eng. J.* 2024, 488, 150566.
- (72) Cameron, J.; Kanibolotsky, A. L.; Skabara, P. J. Lest we forget—the importance of heteroatom interactions in heterocyclic conjugated systems, from synthetic metals to organic semiconductors. *Adv. Mater.* **2023**, 2302259.
- (73) Conboy, G.; Spencer, H. J.; Angioni, E.; Kanibolotsky, A. L.; Findlay, N. J.; Coles, S. J.; Wilson, C.; Pitak, M. B.; Risko, C.; Coropceanu, V.; Brédas, J. L.; et al. To bend or not to bend—are heteroatom interactions within conjugated molecules effective in dictating conformation and planarity? *Mater. Horiz.* **2016**, *3*, 333—339.
- (74) Thorley, K. J.; McCulloch, I. Why are S-F and S-O non-covalent interactions stabilising? *J. Mater. Chem. C* **2018**, *6*, 12413–12421.
- (75) Kharandiuk, T.; Hussien, E. J.; Cameron, J.; Petrina, R.; Findlay, N. J.; Naumov, R.; Klooster, W. T.; Coles, S. J.; Ai, Q.; Goodlett, S.; Risko, C.; et al. Noncovalent Close Contacts in Fluorinated Thiophene—Phenylene—Thiophene Conjugated Units: Understanding the Nature and Dominance of O··· H versus S··· F and O··· F Interactions with Respect to the Control of Polymer Conformation. *Chem. Mater.* **2019**, *31*, 7070—7079.
- (76) Reichenbächer, K.; Süss, H. I.; Hulliger, J. Fluorine in crystal engineering—"the little atom that could. *Chem. Soc. Rev.* **2005**, *34*, 22–30.
- (77) Jackson, N. E.; Savoie, B. M.; Kohlstedt, K. L.; Olvera De La Cruz, M.; Schatz, G. C.; Chen, L. X.; Ratner, M. A. Controlling conformations of conjugated polymers and small molecules: The role of nonbonding interactions. *J. Am. Chem. Soc.* **2013**, *135*, 10475—10483.

(78) Yin, H.; Chen, J.; Zheng, D. Effect of Molecular Substitution and Isomerization on Charge-Transport Parameters in Molecular Organic Semiconductors. *J. Phys. Chem. Lett.* **2021**, *12*, 2660–2667. (79) Thorley, K. J.; Risko, C. On the impact of isomer structure and packing disorder in thienoacene organic semiconductors. *J. Mater. Chem. C* **2016**, *4*, 4040–4048.